



Two-dimensional continuous wavelet transform of simulated spatial images of waves on a slowly varying topography

Laurence Zsu-Hsin Chuang^a, Li-Chung Wu^{a,*}, Dong-Jiing Doong^b, Chia Chuen Kao^a

^a National Cheng Kung University, No. 1, University Road, Tainan, Taiwan, ROC

^b National Taiwan Ocean University, No. 2, Pei-Ning Road, Keelung, Taiwan, ROC

ARTICLE INFO

Article history:

Received 22 September 2007

Accepted 27 February 2008

Available online 7 March 2008

Keywords:

Inhomogeneous wave field

Simulation

Spatial image

Two-dimensional continuous wavelet transform

ABSTRACT

The wavelet transform (WT) is now recognized as a useful, flexible, and efficient technique to analyze intermittent, non-stationary and inhomogeneous signals as well as images which are obtained from experimental or in situ measurements. In this study, the two-dimensional continuous wavelet transform (2-D CWT) was introduced to analyze the spatial image of waves. The numerical algorithm of 2-D CWT was developed and testified in simulated wave field of regular and random waves. Some more simulated wave fields of various wave conditions and sea bed slopes were then assumed to verify the analytical accuracy of this new technique. The comparisons of estimations to theoretical values for several wave parameters show that the 2-D CWT is capable of identifying the directional spectra and wave properties in shallow water.

© 2008 Elsevier Ltd. All rights reserved.

1. Introduction

Ocean waves have attracted considerable attentions throughout history. In the present day, the mechanism of wave formation and the way that waves travel across the coastal ocean is still not fully understood. Wave measurements always play an important role on evaluating and describing wave characteristics. It can be broadly classified into two categories: in situ measurement and remote sensing. Most in situ measurements record time variation of waves at fixed points, nevertheless remote sensing focuses on spatial distinction over a broader area. Many studies on applying remote sensing to ocean wave measurement have been done since the 1960s (Pidgeon, 1968; Valenzuela and Laing, 1970; Alpers and Rufenach, 1981; Lee et al., 1996). Land-based radar is one of prevalent systems on observing ocean waves and has been shown that it is possible to obtain reliable data of wave characteristics after comparing with corresponding buoy data (Borge and Soares, 2000).

In order to derive wave information from radar images, the temporal and spatial evolution of the radar backscatter information of the sea surface were analyzed by means of a Fourier transform (FT) analysis, where spatial homogeneity and temporal stationarity within the observed area and period were assumed. However, it is a fact that most real signals in nature are non-stationary and inhomogeneous; so are wave signals. That is, the

statistical properties of a wave field covered with a wide range frequency and wavenumber components always change with time and space. Obviously, the FT is not acceptable to be employed in analyzing such signals, because it does not possess the property of locality inherent to these signals. Comparatively, the wavelet transform (WT) adopts localized functions to better reflect the properties of time- and space-dependent signals.

The WT is now recognized as a useful, flexible, and efficient technique to analyze intermittent, non-stationary and inhomogeneous signals as well as images which are obtained from experimental or in situ measurements. It has been applied to solve a variety of engineering problems and almost every corner of physics. However, the implementations of WT in one dimension (signal analysis) and in two dimensions (image processing) are quite different. Massel (2001) revealed that WT is capable of analyzing one-dimensional wave signals. Carlson (1995) applied two-dimensional WT to reduce noise and enhance the appearance of individual wave structures in a SAR image of the ocean surface. Niedermeier et al. (2002) used a wavelet edge detection method on the SAR image and used a region-growing approach to examine the wave groupiness.

It is the purpose of this article to develop a procedure for implementing the two-dimensional continuous WTs (2-D CWT) for the applications of digital radar image analysis. In those applications, the wavenumber spectra representing each spatial wave field should be first derived by 2-D CWT, because they are one of the useful ways to describe wave features in the spatial frequency domain (Doong et al., 2003). For examples, the wave directional distribution, wave height, wavelength (wavenumber),

* Corresponding author. Tel.: +886 6 2364492; fax: +886 6 2364519.

E-mail address: jackalson18@gmail.com (L.-C. Wu).

wave period as well as frequency spectrum, transformed from the wavenumber spectrum based on the linear wave theory (Borge and Soares, 2000), could then be derived. In this paper we only discussed the accuracy variations of estimated wave directions and wavenumbers which were figured out by 2-D CWT at different locations of wave field on a slowly varying topography.

2. Theoretical preliminaries

A series $\{X_t\}$ is called ‘stationary’ if its statistical properties do not change with time (Priestley, 1991). For a more precise definition, $\{X_t\}$ is said to be completely stationary if the joint probability distribution of $\{X_{t_1}, X_{t_2}, \dots, X_{t_n}\}$ is identical to that of $\{X_{t_1+k}, X_{t_2+k}, \dots, X_{t_n+k}\}$. Similarly, ‘homogeneity’ implies that the statistical properties do not change with space. The FT can then be applied to those signals or images, but it loses the capability of describing all information about the time/space localization of a

given component. It does not even mention to apply the FT to wave analysis in non-stationary or/and inhomogeneous situations. However, this is the problem we always meet when the land-based radar is chosen to detect the wave features. Nowadays, the FT has been popularly adopted in image analysis by most of the commercial radar monitoring systems, but it may be inadequate to describe the whole wave field by only one representing wavenumber spectrum. Therefore, we developed a new tool, based on 2-D CWT, to identify the transition of wavenumber spectra within a wave field.

There are two essentially different approaches in WT, namely, the continuous WT (CWT) and the discrete WT (DWT). The CWT plays the same role as the FT and is mostly used for analysis and feature detection in signals, whereas the DWT is the analog of the Discrete Fourier Transform and is more appropriate for data compression and signal reconstruction (Antoine et al., 2004). In this paper we used the CWT to detect certain wave characteristics from a single radar image and to represent its wave field locally in

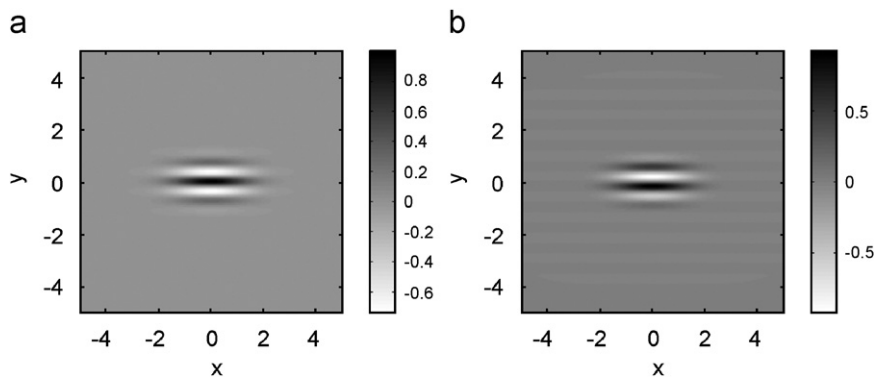


Fig. 1. Morlet mother wavelet function shown in space domain in which the parameter $\vec{k}_0 = (6, 0)$ controls the oscillation of wavelet function: (a) real part and (b) imaginary part.

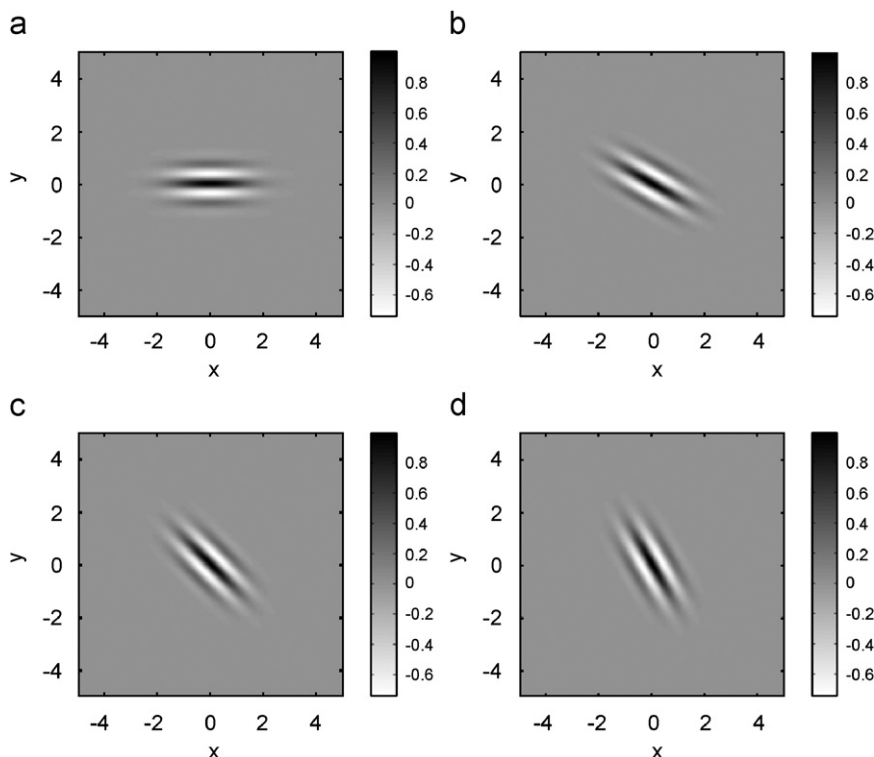


Fig. 2. The real part of Morlet wavelet functions shown in space domain. They are influenced by the rotation matrix r_θ at the angle: (a) $\theta = 0^\circ$, (b) $\theta = 30^\circ$, (c) $\theta = 45^\circ$, and (d) $\theta = 60^\circ$.

both space domain and spatial frequency domain where the wavenumber in analysis can be changed continuously when rescaling.

2.1. Two-dimensional continuous wavelet transform

WT is similar to FT in that it breaks signals into their constituents. However, FT of wave image may wrongly estimate the original information of space when wave length variances are not homogenous in the area of interest; wave length changes in space or has a discontinuity at a specific spot, for examples. That is because the FT yields information on how much but not where (in space) the specific wavenumber components exist. WT, on the other hand, shows more comprehensive changes not only at spatial frequency domain but at space domain. It breaks the image into various wavelets which are scaled and shifted versions of a pre-chosen mother wavelet and allows exceptional localization both in the space domain via translations of the mother wavelet, and in the scale (spatial frequency) domain via dilations and rotations.

Given a two-dimensional spatial image $s(\vec{x}) = s(x,y)$ of finite energy, we could represent the image by

$$\|s\|^2 = \int_{R^2} |s(\vec{x})|^2 d^2 \vec{x} < \infty. \tag{1}$$

It means a complex-valued function defined on the real plane R^2 is square integrable. In practice, a black and white image $s(\vec{x})$ will be

represented by a bounded non-negative function. The discrete values of $s(\vec{x})$ correspond to the level of gray of each pixel (Antoine et al., 2004).

The corresponding CWT of $s(\vec{x})$ with respect to a transformed mother wavelet $\Psi_{b,\theta,a}^-$ is

$$S(\vec{b}, \theta, a) = \frac{1}{\sqrt{C_\Psi}} \langle \Psi_{b,\theta,a}^- | s(\vec{x}) \rangle \tag{2}$$

in which the complex-valued function $\Psi_{b,\theta,a}^-$, localized in space, must satisfy the admissibility condition:

$$C_\Psi = (2\pi)^2 \int_{R^2} \frac{|\hat{\Psi}(\vec{k})|^2}{|\vec{k}|^2} d^2 \vec{k} < \infty \tag{3}$$

where $\hat{\Psi}$ is the FT of Ψ and \vec{k} is the spatial frequency.

Eq. (2) can also be expressed as:

$$S(\vec{b}, \theta, a) = C_\Psi^{-1/2} a^{-1} \int_{R^2} \Psi^*(a^{-1} r_{-\theta}(\vec{x} - \vec{b})) s(\vec{x}) d^2 \vec{x} \tag{4}$$

where Ψ^* is the complex conjugate of the wavelet function Ψ . The scaling parameter a , a nondimensional scale factor, is related to the dilated spatial frequency (wavenumber) of the space domain. The factor a^{-1} is a normalization which gives all dilated versions of the mother wavelet the same energy, i.e., it is the ratio of the size of the dilated wavelet to the size of the mother wavelet. The translation parameter b corresponds to the position of the wavelet as it shifts through the space domain. The rotation matrix r_θ with a rotation angle θ , which rotates the wavelet in spatial coordinates, is usually defined as:

$$r_{-\theta} = \begin{pmatrix} \cos \theta & \sin \theta \\ -\sin \theta & \cos \theta \end{pmatrix}, \quad 0 \leq \theta < 2\pi \tag{5}$$

To implement Eq. (4), we must choose a mother wavelet function Ψ first. Since the wave information detected from radar image is directional, an oriented or directional mother wavelet must be used such as the well-known and most commonly used Morlet wavelet. It is a directionally selective and complex-valued wavelet function and has been popularly adopted in WT for signal analysis (Barache et al., 1997) as well as ocean signal analysis (Chien et al., 2002; Huang, 2004). Thus, a two-dimensional Morlet mother wavelet function, defined in Eq. (6), and its function in Fourier space, defined in Eq. (7) (Mujica, 1999), were used throughout the implementation procedures in this study.

$$\Psi(\vec{x}) = e^{-0.5|A\vec{x}|^2} e^{i(\vec{k}_0 \times \vec{x})} - e^{-0.5|A\vec{x}|^2} e^{(-0.5|A^{-1}\vec{k}_0|^2)} \tag{6}$$

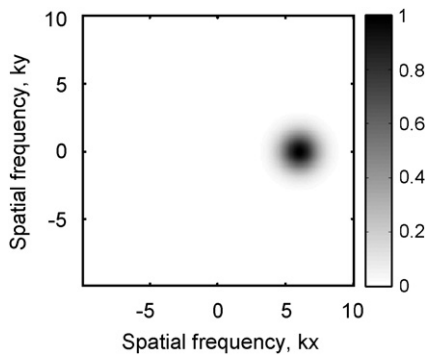


Fig. 3. Morlet mother wavelet function in spatial frequency domain. The energy peak locates at $(k_x, k_y) = (6, 0)$, because the parameter $k_0 = (6, 0)$ is assumed in this case.

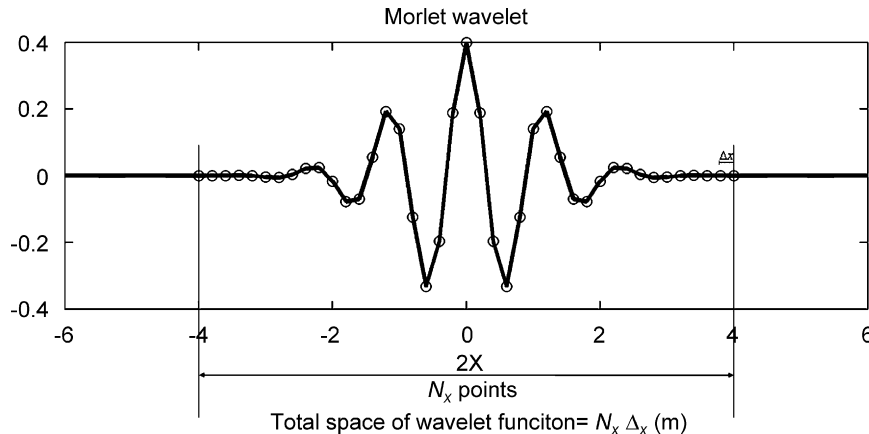


Fig. 4. Relationships between measured spatial samples and wavelet function samples. N_x represents the measured fluctuation sample points and Δx is sampling space (Jordan Jr., 1998).

$$\hat{\psi}(\vec{k}) = \sqrt{\varepsilon} [e^{-0.5|A^{-1}(\vec{k} - \vec{k}_0)|^2} - e^{(-0.5|A^{-1}\vec{k}_0|^2)} e^{-0.5|A^{-1}\vec{k}|^2}] \quad (7)$$

where the parameter \vec{k}_0 is a vector constant that forces the admissibility condition to be satisfied. It can be found that the second terms in Eqs. (6) and (7) could be negligible if $|\vec{k}_0|$ is large enough. Most of cases \vec{k}_0 is chosen in the range between (5,0) and (6,0). The matrix $A = \text{diag}[\varepsilon^{-0.5}, 1]$, in which $\varepsilon \geq 1$, is an anisotropy matrix. The Morlet wavelet is a direction oriented complex function. Its real and imaginary parts are shown in Fig. 1. Its direction is influenced by r_θ as shown in Fig. 2 to extract each wave component direction. The distribution of Morlet wavelet in the spatial frequency domain is illustrated in Fig. 3.

2.2. Basic properties of the 2-D WT implementation

There are several algorithms to implement Eq. (4). The simplest method is direct numerical integration. The drawback is that it is time-consuming. A better solution is to calculate the 2-D CWT results in Fourier (spectral) space, so Eq. (4) could be calculated in another expression:

$$S(\vec{b}, \theta, a) = C_\psi^{-1/2} a \int_{R^2} \hat{\Psi}^*(a r_{-\theta}(\vec{k})) e^{i\vec{b} \cdot \vec{k}} \hat{s}(\vec{k}) d^2 \vec{k} \quad (8)$$

in which $\hat{s}(\vec{k})$ is the FT of $s(\vec{x})$

$$\hat{s}(\vec{k}) = \hat{s}(k_x, k_y) = (2\pi)^{-1} \int_{R^2} s(\vec{x}) e^{-i(\vec{k} \cdot \vec{x})} d^2 \vec{x} \quad (9)$$

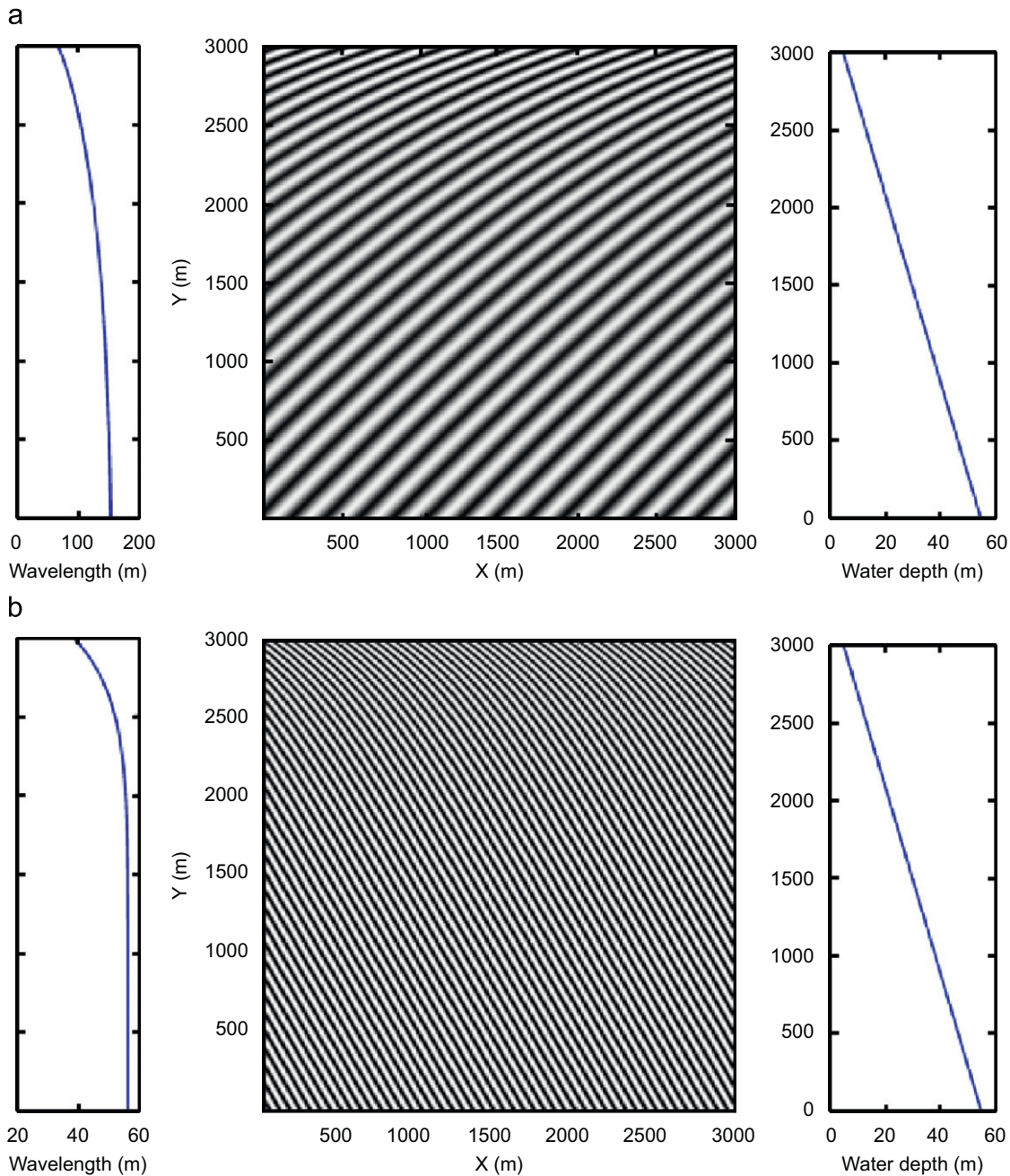


Fig. 5. Simulated wave field of regular waves in water of varying depth contour parallel to the coast: (a) a swell field and (b) a wind wave field. Due to water depth variation, the wavelengths get decreasing in shallow water area and the decreasing rates of swell and wind wave are different.

\vec{k} is the spatial frequency, i.e., the wave number of ocean wave, and $\hat{\Psi}_{b,\theta,a}^-(k)$, the FT of $\Psi_{b,\theta,a}^-(\vec{x})$, is defined as:

$$\hat{\Psi}_{b,\theta,a}^-(k) = ae^{-i\vec{b}\cdot\vec{k}}\hat{\Psi}(ar_{-\theta}(k)) \quad (10)$$

To better explain the results obtained from image processing by 2-D CWT technique, we need to interpret some basic properties in some detail. Eq. (10) shows that the spatial frequency could be transformed from k into $ar_{-\theta}(k)$ after scaling, shifting and rotating a wavelet. As shown in Eq. (7), k_0 is the spatial frequency, where the peak energy locates, of the mother Morlet function in Fourier space. After transforming, a new location of the peak energy of the Morlet wavelet function in Fourier space becomes \vec{k}_n . The relationship between \vec{k}_0 and \vec{k}_n is given as:

$$\vec{k}_n = \frac{\vec{k}_0}{ar_{-\theta}} \quad (11)$$

On combining the relationship in Eq. (11) and specifying a value for the shifting parameter b in Eq. (10), we could applied the 2-D WT to a radar image of ocean waves to recognize the wave energy change for each wavenumber component at different positions of wave field.

The wave image for analyzing is always in a digital form. In order to use the framework of continuous wavelets to analyze discretely sampled data, it is necessary to sample the analyzing wavelet (Jordan et al., 1997). A simplified example as shown in Fig. 4 could be introduced to explain the idea. A physical space series has sampling space Δx m and total number of sample points N_x . The total length to be transformed by a 1-D mother wavelet is $N_x\Delta x$ m. The total nondimensional length of mother wavelet is $2X$; it is mapped for N_x points. The correspondence between the dimensional and nondimensional sampling spaces can be obtained through the relationship (Jordan Jr., 1998):

$$[-X, X] \leftrightarrow [0, N_x\Delta x] \quad (12)$$

Considering the influence of discretely sampled data, Eq. (11) becomes

$$\vec{k}_n = \frac{\vec{k}_0}{ar_{-\theta}} \times \frac{2X}{N_x\Delta x} \quad (13)$$

Hence, Eq. (8) could be expressed in the function of \vec{x} and \vec{k}_n , as

Eq. (14), after applying the discretely continuous WT on the digital wave images:

$$S(\vec{b}, \theta, a) \rightarrow S(\vec{x}, \vec{k}_n) \quad (14)$$

in which, the corresponding wavenumber \vec{k}_n is influenced by the scaling and rotation of the mother wavelet. The energy distribution $S(\vec{x}, k_n)$, representing the wavenumber spectrum $S(k_n)$ at different spatial locations \vec{x} , is the results that we want to obtain from the wave field.

3. Wave field image simulation and analysis

To examine the validity of the new technique presented above and to test the algorithm of computing the 2-D CWT, the following numerical simulations of wave field images with incident, refracted and reflected waves in water of varying depth were performed and discussed.

3.1. Simulation and analysis of wave image of the superposition of regular waves

A regular wave, propagating along a single direction in the space domain, could be given by

$$\eta(x, y) = a \cos(k \cos \alpha x + k \sin \alpha y) \quad (15)$$

in which a is the wave amplitude, k the wavenumber, and α the wave direction. Eq. (15) describes the simplest regular wave. Due to the influences of water depth and coastal structures, waves would be transformed. Waves that encounter a solid vertical surface (such as a seawall) will abruptly change their directions. Sometimes reflection can create very dangerous conditions when the reflected waves interfere constructively with the incoming waves. Waves propagating at shallow water regions gradually change in height as a result of the change in the rate of the energy flux due to a reduction in the water depth. Waves may also bend if they approach the beach in an incident angle.

The equations to simulate wave fields influenced by reflection, refraction and shoaling are given as (Chang and Hsu, 2003; Chang,

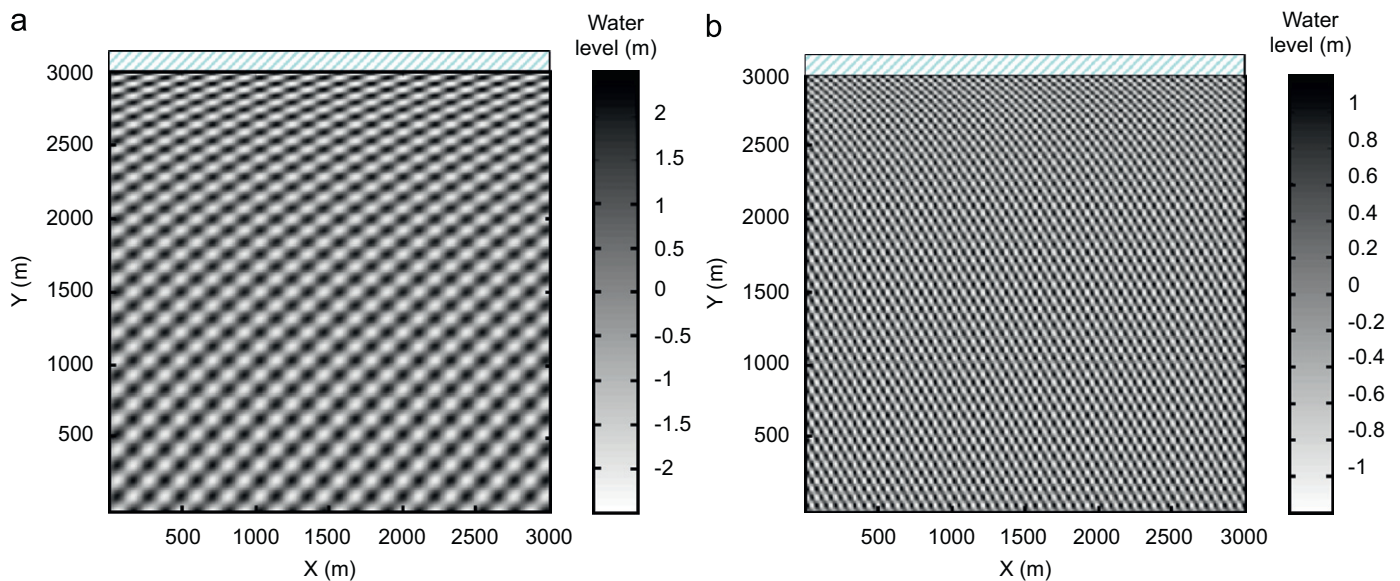


Fig. 6. Simulated wave images of incident and reflected regular waves in water of varying depth contour parallel to the coast: (a) swell and (b) wind waves.

2002; Horikawa, 1988)

$$\eta(x, y) = a_i[\cos(A + \varepsilon_i) + K_R \cos(A + \varepsilon_i + \varepsilon_r)]$$

$$a_i = a_0 \times K_s$$

$$K_s = \left[\tanh(kh) + \frac{kh}{\cosh^2(kh)} \right]^{-0.5}$$

$$(16) \quad A = \int_0^x (k \cos \theta) dx + k \sin \theta y$$

$$(17) \quad \omega = \sqrt{gk \tanh(kh)}$$

(18)

in which parameters k and a were defined in Eq. (15). K_s is the shoaling coefficient, K_R the reflection coefficient, ε_i the phase of the incident waves, ε_r the phase of the reflected waves, a_i the

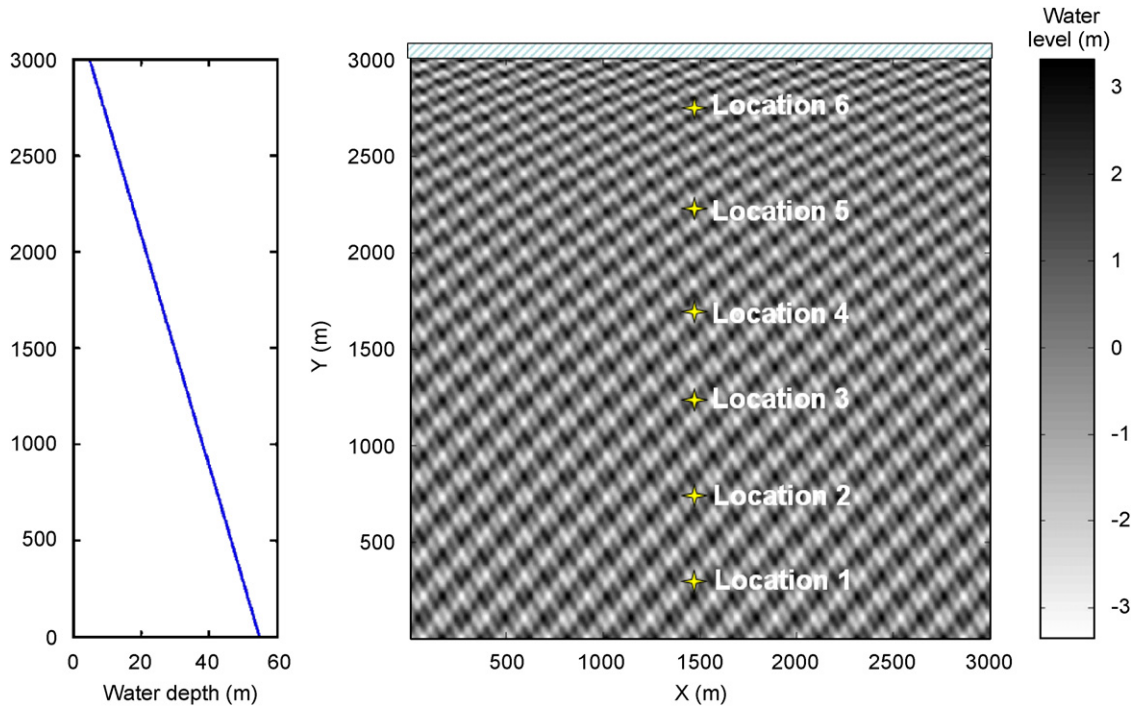


Fig. 7. Simulated wave images of four regular wave components, including incident swell, incident wind waves, reflected swell and reflected wind wave, which are in water of varying depth contour parallel to the coast. Six spatial locations in the wave field were chosen to execute 2-D CWT.

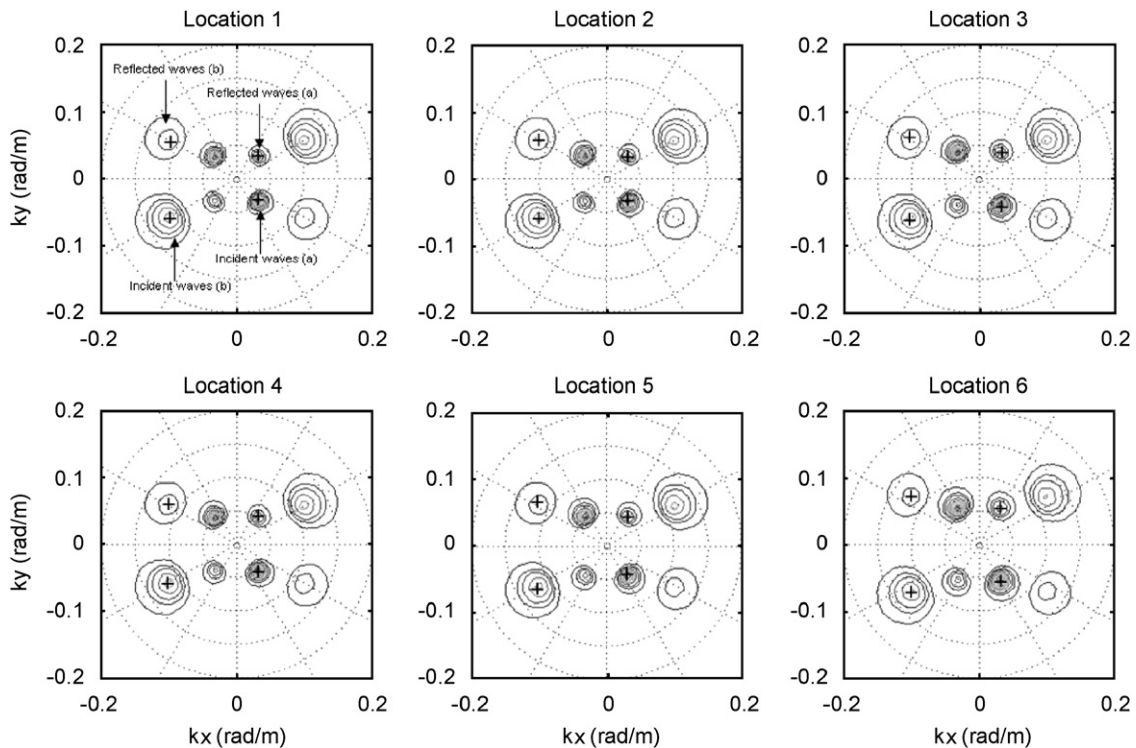


Fig. 8. Wavenumber energy contours, which are projected shadows of wavenumber spectra on the wavenumber plane, estimated by 2-D CWT at six locations of the wave field image of regular waves. The theoretical wavenumbers are marked by the plus signs.

amplitude of incident waves, and h the water depth. According to linear wave theory, wave period keeps constant when a train of simple harmonic wave moves in the region of gradually decreasing water depth. The wavenumber, derived from the relationship in Eq. (20) at different water depths, can then be substituted into Eq. (18) and Eq. (19).

A swell system with wave height = 3 m, incident wave direction = 135°, and wave period = 10 s at deepest water depth was simulated to propagate in water of varying depth contour parallel to the coast. The wave field transaction is illustrated in Fig. 5(a). Another wind wave system with wave height = 1.6 m, incident wave direction = 240°, and wave period = 6 s at deepest water depth was also simulated to propagate into shallow water. The wave field transaction is illustrated in Fig. 5(b). According to wave theory, the wavelength decreases due to shallow water depth. Both Fig. 5(a) and (b) did show that longer waves appear at deeper water depths.

If a solid structure lies to the north of wave field and the reflection coefficient is $K_R = 0.5$, these new conditions will make the two above-mentioned wave systems more complicated as shown in Fig. 6(a) and (b), respectively. In consideration of two wave systems coexist in the same field as well as the effects of refraction and reflection, two wave fields in Fig. 6(a) and (b) could be superimposed to become a new wave field as demonstrated in Fig. 7. The wave fields will consist of an incident swell, its reflected component, an incident wind wave, its reflected component, and the shoaling effects on each component. This case was analyzed

by the 2-D CWT to justify the validity and accuracy of the method and algorithm.

The wavenumber spectra estimated by 2-D CWT at different locations, marked in Fig. 7, project shadows on the wavenumber plane to become wavenumber energy contours as shown in Fig. 8. Each contour corresponds to one wave component and its mirror one in opposite direction. It means the wave directions are ambiguous in judging the 180° difference when a single wave image is transformed for wavenumber spectrum. The ambiguity could be eliminated by adopting a series of wave images. There are four pairs of energy contours corresponding to one incident swell, its reflected component, one incident wind wave, and its reflected component at each location. The spectral energy at the higher wavenumber is more scattered than that at the lower wavenumber. This is because the higher wavenumber component has lower resolution in spatial frequency and higher resolution in space domain. This is known as the Heisenberg Uncertainty Principle (Van Name, 1960).

Fig. 8 shows that the estimated wavenumber and the estimated dominant wave direction for each wave component gradually change at different locations of field. Obviously this is due to wave refraction. It also shows that the estimated wavenumber and direction at each peak of energy contour, representing each single harmonic wave, are consistent with the theoretical values marked by the plus signs. The simulation, analysis, and discussion above proved that 2-D CWT is a practicable technique for analyzing wave field image of regular waves.

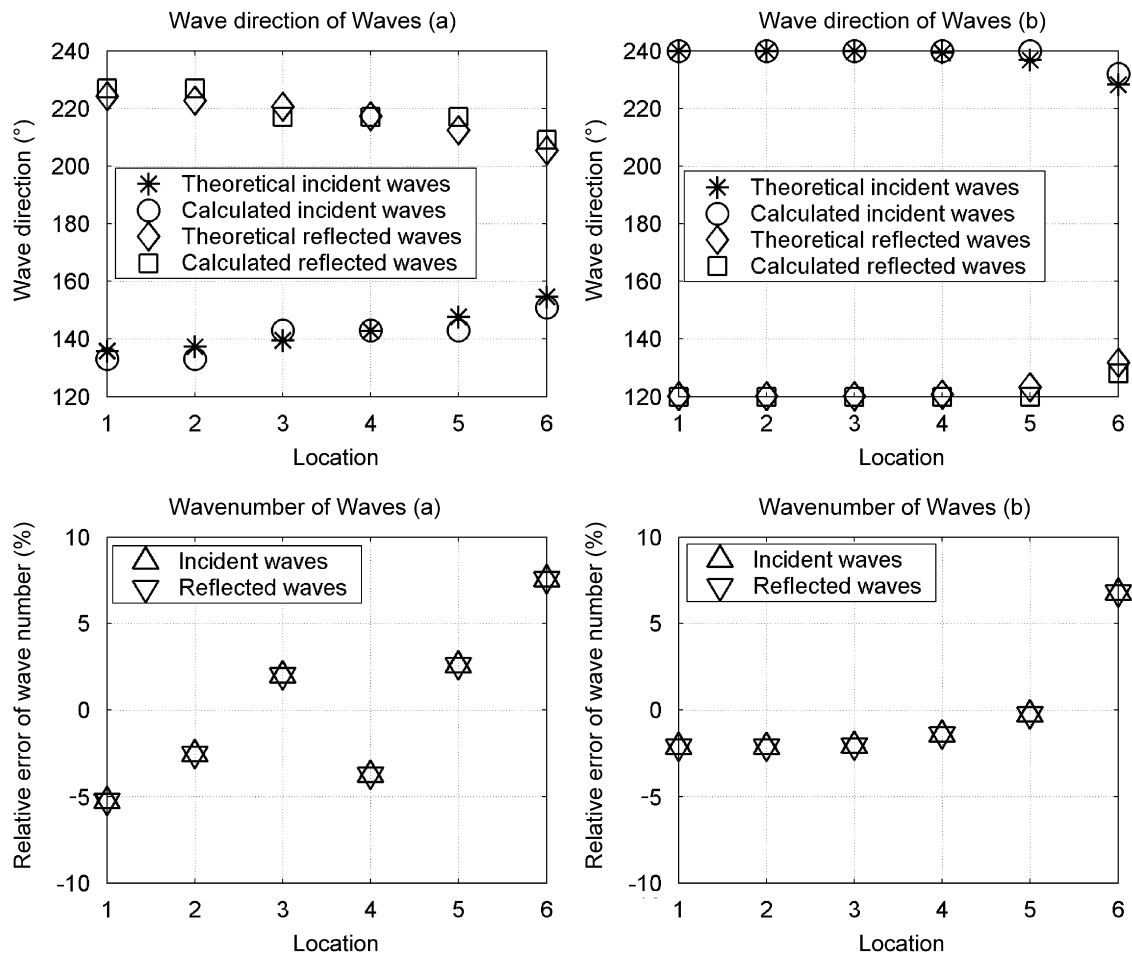


Fig. 9. Accuracy comparison of theoretical values to estimated values of wave directions and wavenumbers which were derived from 2-D CWT results at different locations.

To distinguish the capability and evaluate the accuracy of 2-D CWT, we compared the theoretic values to calculated values of four wave components at six locations of various water depths. The comparison is shown in Fig. 9. A reasonably good agreement is observed for incident swell and wind waves as well as for their reflected ones when they propagate into shallow water. The relative errors in wavenumber estimation are less than 5%, except for the analyzing locations near the edge of image. The discussion above demonstrates that the 2-D CWT has high accuracy power and capably separates incident and reflected wave components.

3.2. Simulation and analysis of random wave field image

Ocean waves in nature are random, not regular. The 2-D CWT algorithm developed above need to be justified in the random wave field. Hence, several numerical simulations were carried out for random wave fields, in which a directional spectrum was assumed.

The full directional spectrum can be represented by (Tucker and Pitt, 2001)

$$S(f, \theta) = S(f) \times G(f, \theta) \tag{21}$$

where $S(f)$ is the one-dimensional spectrum; $G(f, \theta)$ is the directional spreading function which expresses how the energy at frequency f is distributed by direction of travel.

To simulate the irregular waves propagating in varying water depths, we chose a TMA-type spectrum for further study. The one-dimensional spectrum for simulation is defined in Eqs. (22)–(28) (Goda, 1999):

$$S(f) = \phi(kh) \times S_j(f) \tag{22}$$

$$\phi(kh) = \frac{\tanh^3(kh)}{\tanh(kh) + (kh) - (kh)\tanh^2(kh)} = \frac{\tanh^2(kh)}{1 + (2kh)/\sinh(2kh)} \tag{23}$$

$$S_j(f) = \beta_j H_{1/3}^2 T_p^{-4} f^{-5} \exp[-1.25(T_p f)^{-4}] \gamma \exp[-(f/f_p - 1)^2 / 2\sigma^2] \tag{24}$$

$$f_p = \frac{1}{T_p} \tag{25}$$

$$\sigma = \begin{cases} 0.07 & f \leq f_p \\ 0.09 & f > f_p \end{cases} \tag{26}$$

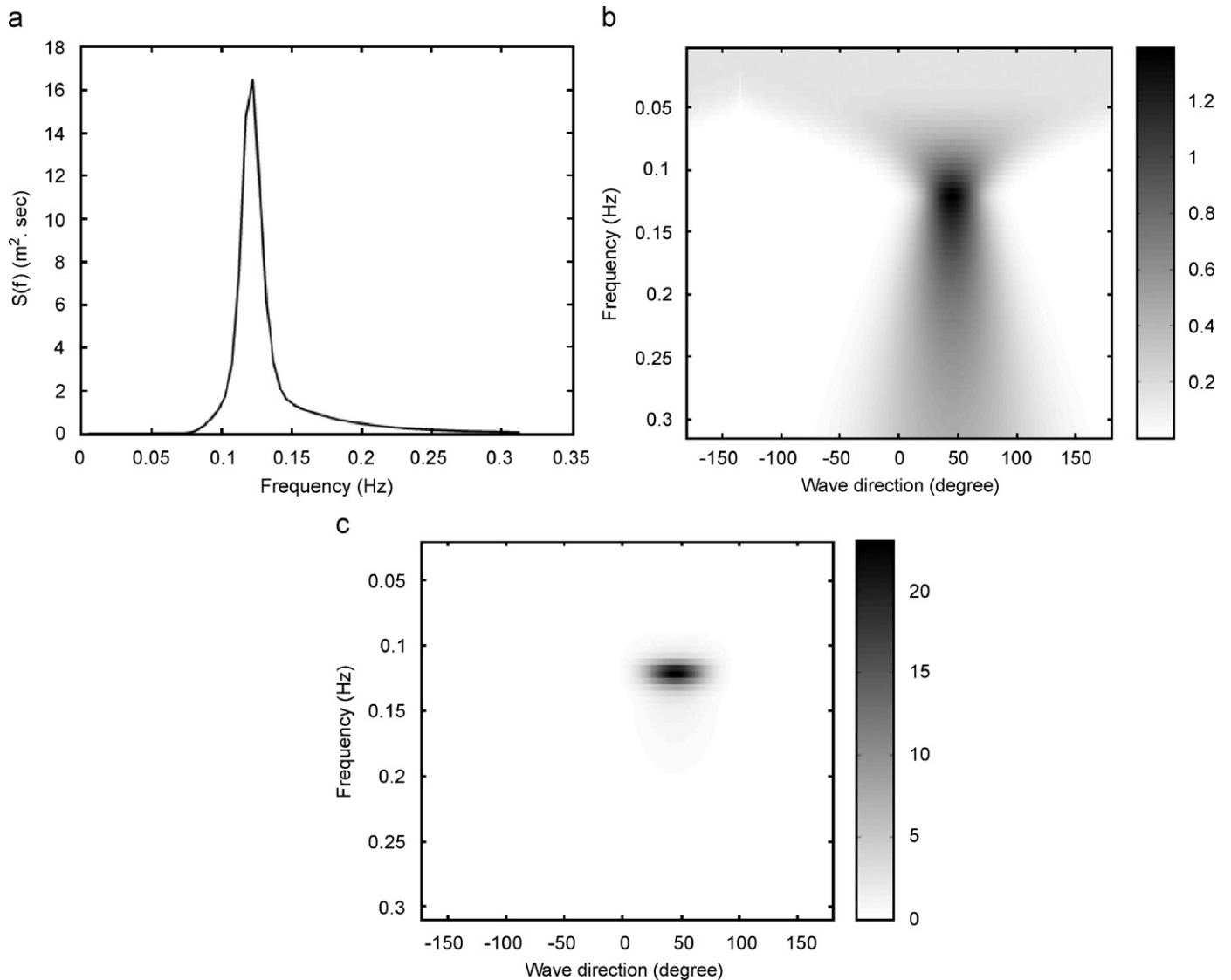


Fig. 10. Simulated random wave spectrum: (a) 1-D wave spectrum, (b) directional spreading function, and (c) directional wave spectrum.

$$\beta_j = \frac{0.0624}{0.230 + 0.0336\gamma - 0.185(1.9 + \gamma)^{-1} \times [1.094 - 0.01915 \ln \gamma]} \quad (27)$$

$$T_p = \frac{T_{H_{1/3}}}{1 - 0.132(\gamma + 0.2)^{-0.559}} \quad (28)$$

A Mitsuyasu-type directional distribution was adopted and defined as:

$$G(f, \theta) = G_0 \cos^{2s} \left[\frac{\theta - \theta_p}{2} \right] \quad (29)$$

$$\int_{-\pi}^{\pi} G(f, \theta) d\theta = 1 \quad (30)$$

$$G_0 = \frac{1}{\pi} 2^{2s-1} \frac{\Gamma^2(s+1)}{\Gamma(2s+1)} \quad (31)$$

$$s = \begin{cases} s_{\max} \left(\frac{f}{f_p}\right)^5 & f \leq f_p \\ s_{\max} \left(\frac{f}{f_p}\right)^{-2.5} & f > f_p \end{cases} \quad (32)$$

- $S_{\max} = 10 \leftarrow$ wind waves
 - $S_{\max} = 25 \leftarrow$ swell with short decay distance
 - $S_{\max} = 75 \leftarrow$ swell with long decay distance
- (33)

where θ_p is the dominant wave direction. The parameter s controls the angular distribution of waves and is known to vary with respect to frequency. The spreading parameter S_{\max} changes with wave conditions as described in Eq. (33).

The irregular wave field can be represented by Eq. (34). The expression is suitable for a sloped sea bed (Horikawa, 1988):

$$\eta(x, y) = a_{mn} \times \sum_{m=-M/2}^{M/2} \sum_{n=1}^N \sin \left(\int_0^x k_m \cos \theta_n dx + k_m \sin \theta_n y + \varepsilon_{mn} \right) \quad (34)$$

in which ε_{mn} is a random phase angle. The amplitude a_{mn} can be derived from the assuming directional spectrum as Eq. (35). The input wavenumber is calculated from the dispersion relationship in Eq. (36):

$$a_{mn} = \sum_{m=-M/2}^{M/2} \sum_{n=1}^N \sqrt{S(\omega_m, \theta_n) \Delta\omega \Delta\theta} \quad (35)$$

$$\omega_m = \sqrt{gk_m \tanh(k_m h)} \quad (36)$$

In simulating a random wave field, a directional spectrum as shown in Fig. 10 was chosen to provide the input condition for Eq. (35). The supposed directional spectrum represents a swell system with significant wave height = 2.5 m, mean wave period = 8 s, dominant wave direction = 45° and $S_{\max} = 25$, i.e., this is a swell field with short decay distance. Assuming this wave system approaches the coast in the water of varying depth contour parallel to the coast line, the simulated wave field image could be illustrated in Fig. 11.

By applying the 2-D CWT to the analysis of simulated random wave field, the 2-D wavenumber spectra for six locations, marked in Fig. 11, were derived and projected on the wavenumber plane to become wavenumber energy contours as shown in Fig. 12. It shows that the wavenumber corresponding to energy contour at

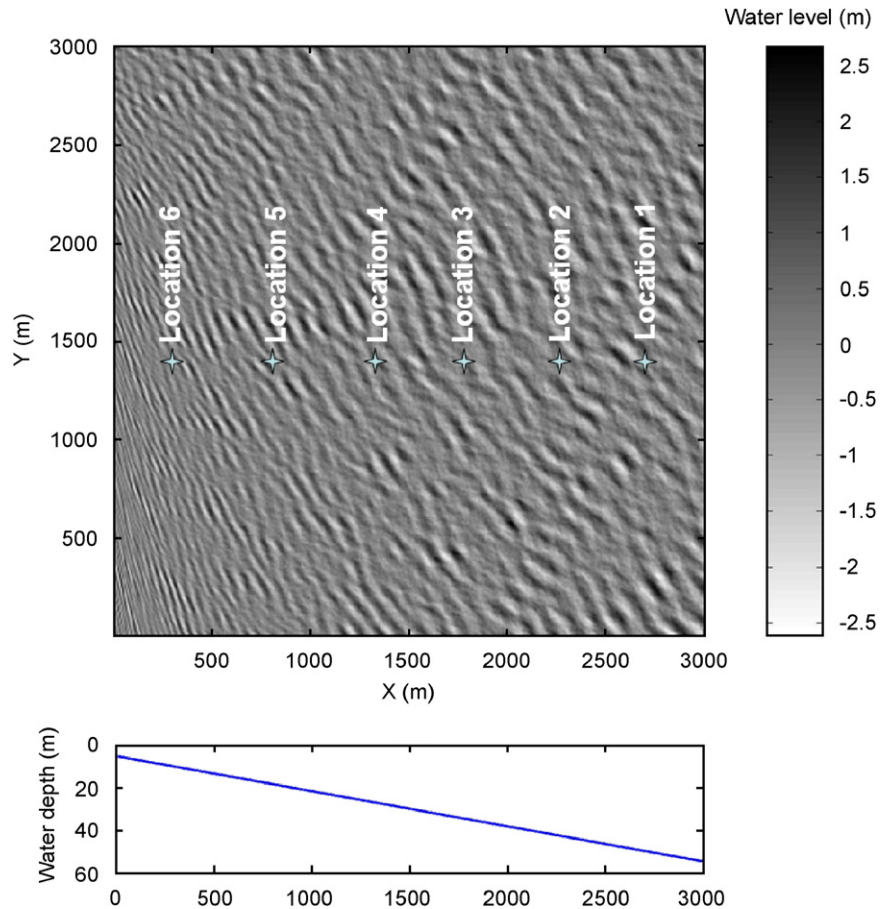


Fig. 11. Simulated random wave field on a sloping varying topography. Six spatial locations were chosen to derive the localized wavenumber spectra.

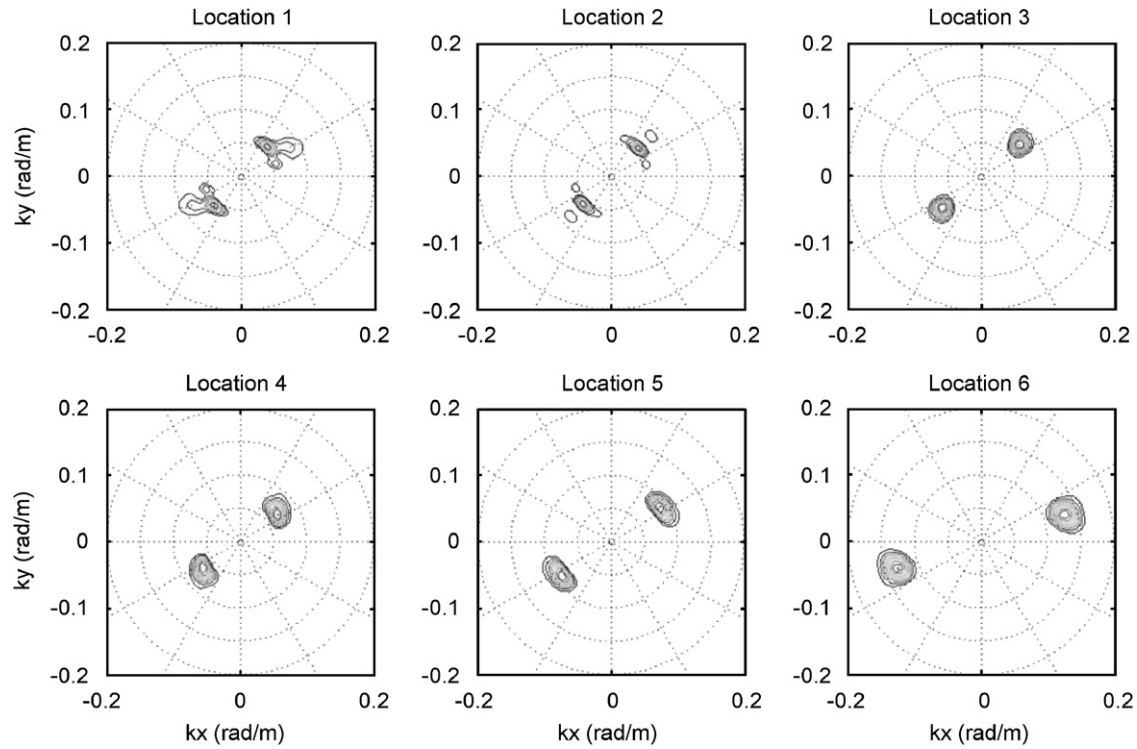


Fig. 12. Wavenumber energy contours estimated by 2-D CWT at six locations of the wave field image of directional random waves.

location 1 (deeper water) gradually moves from a lower value to higher one at location 6 (shallow water), i.e., the wavelengths get shorter as the swell system approaches the coast. The dominant wave directions also change with the water depths.

Since the primary input condition of random wave field simulation is a supposed directional spectrum, the divergence of spectral energy evaluated by 2-D CWT from the theoretical values derived by Eq. (22) should be discussed. A comparison of total energy of each evaluated spectrum (by 2-D CWT) to its theoretical one is shown in Fig. 13. We found that the relative differences between the theoretical values and the wavelet results were less than 10%, except for the locations near the edges of image. These errors might come from the algorithm, in which we discretized the continuous WT on analyzing the digital images. The spatial resolution of wave field image that we measured and the spatial frequency (wavenumber) resolution of 2-D CWT that we chose would affect the accuracy of WT results. Fig. 13 also shows a shortcoming in 2-D CWT analysis. The estimated spectral energy could be influenced by the distance of location from the image edge. The accuracy increases with increasing the distance from the edge.

Fig. 14 shows the comparisons of wavenumbers and wave directions at six different locations. The difference between estimated wavenumbers and theoretical values at different locations are less than 5%, except for the location 1 because of the edge influence. The estimated wave directions are consistent with the theoretic values, except for the location 6 of 5° difference.

All discussions above show that the 2-D CWT is capable of extracting the wavenumber spectrum at any chosen location of the coastal area of varying water depths from an image of random wave field. However, the accuracy could be influenced by the distance from the edge of image. This feature can be explained by Fig. 15. According to Eq. (2), the WT is seen as the inner product of the wavelet function and the image function (wave field). However, the wavelet function is not complete at the locations of interest near the edge of the image, because its energy

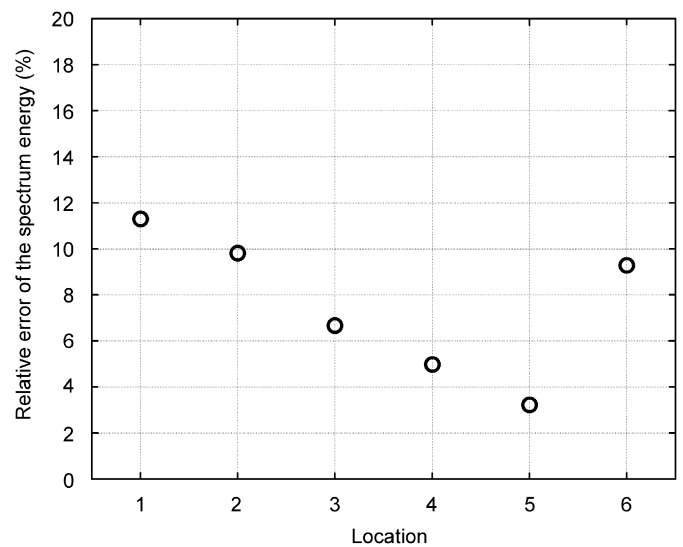


Fig. 13. Relative errors of wavenumber spectral energy between the theoretical values and the evaluations by 2-D CWT at different locations.

distribution is cut off there. After applying this incomplete wavelet function to the wave field, the spectrum energy is biased.

4. Discussion

The wave conditions in the cases discussed above is limit. We need more cases in different wave conditions to verify the practicability and conclusions we have above are generally suitable for use in the future. To simulate a random wave field image, three wave parameters must be assumed, which are wave period, wave height, and wave direction. We presumed different wave conditions of nine wave period ranges from 4 to 12 s as well

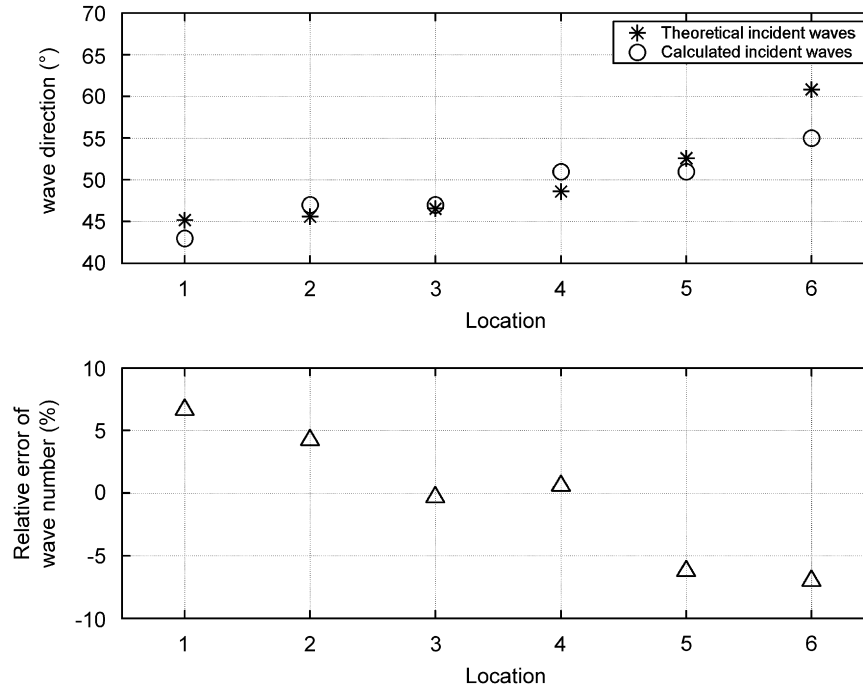


Fig. 14. Comparison of theoretical wave directions and wavenumbers to estimations at six locations.

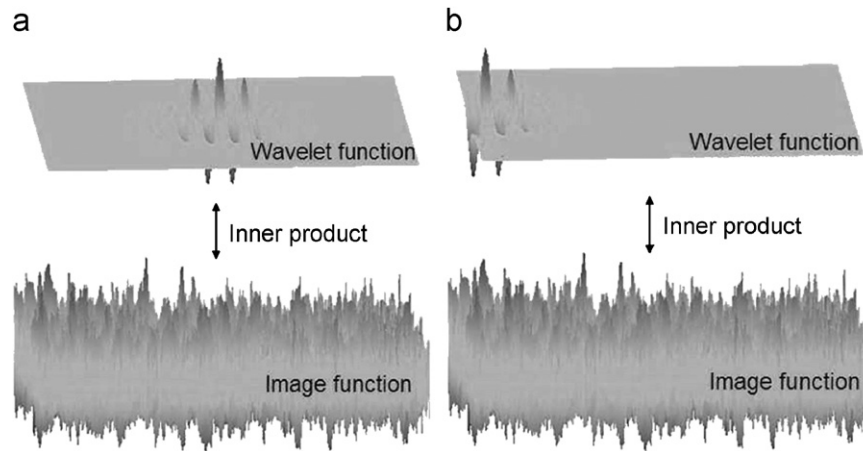


Fig. 15. A schematic illustration of a wavelet function performed on the marginal area of an image function. The inner product of the incomplete wavelet function and the image function provides an incorrect WT energy spectrum.

as constant wave height and wave direction progressing in the same water depth contour. The analyzed results derived by 2-D CWT are shown together in Fig. 16. The influence of different wave periods on the accuracy of detecting wavenumber and wave direction is not so pronounced. The errors in estimating the wave direction are all less than 3° , except the locations near the edge of image. The relative errors in estimating the wavenumber are all less than 5%, except the edge effect, and the accuracy does not obviously change with wave periods and locations. This accuracy level is sufficient to be applied to the analysis in ocean and coastal engineering applications.

In consideration of the refraction effect relying on sea bed slope, we also discussed the influence of different sea bed slopes on estimating wave parameters. We assumed each wave system, in the same wave conditions, travels on different sea bed slopes of 10 ranges from 0.01 to 0.1. The analyzed results derived by 2-D CWT are shown together in Fig. 17. The influence of different sea bed slopes on the accuracy of detecting wavenumber and wave

direction is not so pronounced. The errors in estimating the wave direction are all less than 4° , except the locations near the edges of image. The accuracy does not obviously change with the slope. Most of the relative errors for wavenumber calculation are less than $\pm 5\%$, except the location 6, and the accuracy does not obviously change with the slope, either. The discussion shows that 2-D CWT could be utilized to estimate the directional spectrum and wave parameters in most of coastal area.

5. Conclusions

Ocean wave measurement is a very important research topic in ocean engineering/science. Land-based radar is one of prevailing systems on observing ocean waves and has the capability on obtaining reliable wave information. Nowadays, most of the commercial radar monitoring systems utilize the 2-D FT to analyze the radar images by assuming the wave field is

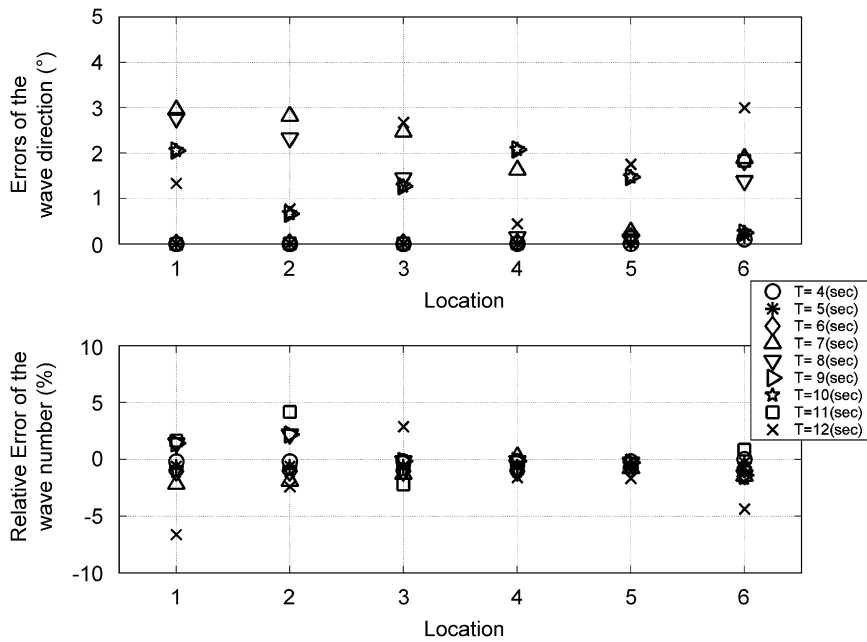


Fig. 16. Estimation errors of wave directions and wave numbers against locations for different wave periods.

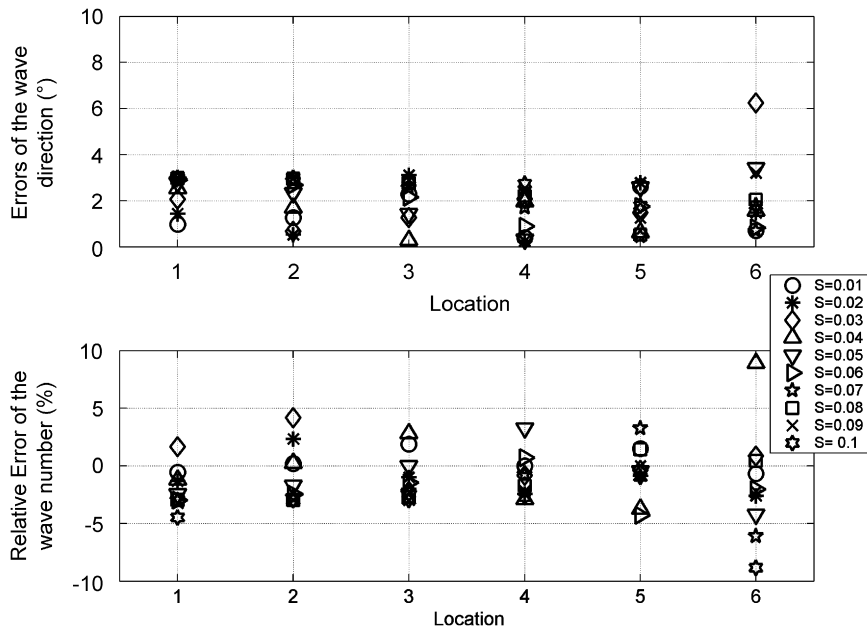


Fig. 17. Estimation errors of wave directions and wave numbers against locations for different sea bed slopes.

homogenous. This assumption may be acceptable in deep water field, but it might mislead the acknowledging of wave features distribution in coastal area or wave–current interaction area. Therefore, a new technique based on the two-dimensional continuous wavelet transform (2-D CWT) was developed in this research to represent a wave field locally in both space domain and spatial frequency domain. The required theories of 2-D CWT were collected, defined and explained how its variables related to ocean waves. The relationship between the energy spectra derived by WT and wavenumber spectra of random waves was then derived.

A spatial image of regular waves was simulated, in which one swell and one wind wave coexist and both waves propagate and reflect in water of varying depth contour parallel to the coastline.

The simulated wave field was then analyzed by 2-D CWT to derive 2-D wavenumber spectra at distinct spatial locations. It shows that the estimated wavenumbers and directions are consistent with the input conditions. The quantitative comparisons also show that the 2-D CWT has high accuracy power and capably separates incident and reflected wave components even in shallow water.

Ocean waves in nature are random. Hence, several numerical simulations were carried out for random wave fields, in which a directional spectrum was assumed, to justify the feasibility of 2-D CWT. We concluded that the 2-D CWT is capable of extracting the wavenumber spectrum at any chosen location of the coastal area of varying water depths from an image of random wave field. And then some more different wave conditions were simulated to

verify the accuracy of 2-D CWT in various sea bed slopes. It shows that the accuracy level is sufficient to apply the 2-D CWT to the analysis on ocean and coastal engineering applications.

This study also shows a shortcoming in 2-D CWT analysis. The estimated spectral energy and the accuracy of detecting wave parameters are influenced by the distance of analyzing location from the image edge. The accuracy increases with increasing the distance from the edge.

Now we could conclude that the feasibility of 2-D CWT on analyzing the wave image of random waves is palpable, even in the coastal area.

References

- Antoine, J.-P., Murenzi, R., Vandergheynst, P., Twareque Ali, S., 2004. *Two-Dimensional Wavelets and their Relatives*. Cambridge University Press, UK.
- Alpers, W., Rufenach, C.L., 1981. On the detectability of ocean surface waves by real and synthetic aperture radar. *Journal of Geophysical Research* 86, 6481–6498.
- Barache, D., Antoine, J.-P., Dereppe, J.-M., 1997. The continuous wavelet transform, an analysis tool for NMR spectroscopy. *Journal of Magnetic Resonance* 128, 1–11.
- Borge, J.C.N., Soares, C.G., 2000. Analysis of directional wave fields using X-band navigation radar. *Coastal Engineering* 40, 375–391.
- Carlson, G.E., 1995. Wavelet processing of SAR ocean wave images. In: *International Geoscience and Remote Sensing Symposium, IGARSS, Firenze, Italy* 1, 679–681.
- Chien, H., Kao, C.C., Chuang, Z.H.L., 2002. On the characteristics of observed coastal freak waves. *Coastal Engineering Journal* 44, 301–319.
- Chang, H.K., 2002. A three-point method for separating of incident and reflected waves over a sloping bed. *China Ocean Engineering* 16, 499–511.
- Chang, H.-K., Hsu, T.-W., 2003. A two-point method for estimating wave reflection over a sloping beach. *Ocean Engineering* 30, 1833–1847.
- Doong, D.J., Kao, C.C., Chuang, Z.H.L., Lin, H.P., 2003. Nearshore wave analysis using SAR images. *China Ocean Engineering* 17 (1), 45.
- Goda, Y., 1999. A comparative review on the functional forms of directional wave spectrum. *Coastal Engineering Journal* 41 (1), 1–20.
- Horikawa, K., 1988. *Nearshore Dynamics and Coastal Processes—Theory, Measurement, and Predictive Models*. University of Tokyo Press, Japan.
- Huang, M.C., 2004. Wave parameters and functions in wavelet analysis. *Ocean Engineering* 31, 111–125.
- Jordan Jr., D.A., 1998. Application of the continuous wavelet transform to science and engineering problems: fluid dynamics case studies. Ph.D. Dissertation, The University of Texas at Austin, USA.
- Jordan, D., Miksada, R.W., Powers, E.J., 1997. Implementation of the continuous wavelet transform for digital time series analysis. *Reviews in Science Instruments* 68 (3), 1484–1494.
- Lee, P.H.Y., Barter, J.D., Caponi, M., Hindman, C.L., Lake, B.M., Rungaldier, H., 1996. Wind-speed dependence of small-grazing-angle microwave backscatter from sea surface. *IEEE Transactions on Antennas and Propagation* 44 (3), 333–340.
- Massel, S.R., 2001. Wavelet analysis for processing of ocean surface wave records. *Ocean Engineering* 28, 957–987.
- Mujica, F.A., 1999. Spatio-temporal continuous wavelet transform for motion estimation. School of Electrical and Computer Engineering Theses and Dissertations Georgia Tech Theses and Dissertations. Georgia Institute of Technology, Georgia, USA.
- Niedermeier, A., Schulz-Stellenfleth, J., Borge, J.C.N., Lehner, S., Dankert, H., 2002. Ocean Wave Groupiness from ERS-1/2 and ENVISAT Images. *International Geoscience and Remote Sensing Symposium, IGARSS, Toronto, Ont., Canada* 2, 928–930.
- Pidgeon, V.W., 1968. Doppler dependence of radar sea return. *Journal of Geophysical Research* 73, 1333–1341.
- Priestley, M.B., 1991. *Non-Linear and Non-Stationary Time Series Analysis*. Academic Press Limited, London, UK.
- Tucker, M.J., Pitt, E.G., 2001. *Waves in Ocean Engineering*. Elsevier Science Ltd., Oxford, UK.
- Valenzuela, G.R., Laing, M.B., 1970. Study of Doppler spectra of radar sea echo. *Journal of Geophysical Research* 75, 551–563.
- Van Name, F.W., 1960. *Modern Physics*. Prentice-Hall Inc., Englewood Cliffs, NJ, USA.